ARO 15365.2-A-E

ADA082004

REPORT DOCUMENTATION PAGE

READ INSTRUCTIONS
BEFORE COMPLETING FORM

1. REPORT NUMBER	2. GOVT ACCESSION NO.	3. RECIPIENT'S CATALOG NUMBER

4. TITLE (and Subtitle) AN INVESTIGATION OF ATMOSPHERIC OPTICALLY SCATTERED NON-LINE-OF-SIGHT COMMUNICATION LINKS	5. TYPE OF REPORT & PERIOD COVERED Final Report, Sept 1978 to Sept 1979
	6. PERFORMING ORG. REPORT NUMBER

7. AUTHOR(s) Submitted by: Warren S. Ross Principal Investigator: Robert S. Kennedy	8. CONTRACT OR GRANT NUMBER(s) DAAG29-77-C-0048

9. PERFORMING ORGANIZATION NAME AND ADDRESS Massachusetts Institute of Technology Research Laboratory of Electronics, Cambridge Massachusetts 02139	10. PROGRAM ELEMENT, PROJECT, TASK AREA & WORK UNIT NUMBERS

11. CONTROLLING OFFICE NAME AND ADDRESS U. S. Army Research Office P. O. Box 12211 Research Triangle Park, NC 27709	12. REPORT DATE January 5, 1980
	13. NUMBER OF PAGES 66

14. MONITORING AGENCY NAME & ADDRESS(if different from Controlling Office)	15. SECURITY CLASS. (of this report) Unclassified
	15a. DECLASSIFICATION/DOWNGRADING SCHEDULE

LEVEL

DTIC
ELECTE
MAR 11 1980
S D

16. DISTRIBUTION STATEMENT (of this Report)

Approved for public release; distribution unlimited.

17. DISTRIBUTION STATEMENT (of the abstract entered in Block 20, if different from Report)

18. SUPPLEMENTARY NOTES

19. KEY WORDS (Continue on reverse side if necessary and identify by block number)

optical scatter propagation
fog, optical properties of
ultraviolet light propagation
non-line-of-sight optical communication

20. ABSTRACT (Continue on reverse side if necessary and identify by block number)

This report discusses the work performed in the second year of a two year program to investigate short-haul non-line-of-sight optical scatter communication links. The wavelength region considered for this study is the middle ultraviolet (uv) (2000 Å - 3000 Å).

DD FORM 1473 EDITION OF 1 NOV 65 IS OBSOLETE
1 JAN 73

FINAL REPORT
(SIXTY COPIES REQUIRED)

1. ARO PROPOSAL NUMBER: _____

2. PERIOD COVERED BY REPORT: <u>September 1978 - September 1979</u>

3. TITLE OF PROPOSAL: <u>An Investigation of Atmospheric Optically</u>

   <u>Scattered Non-Line-of-Sight Communication Links</u>

4. CONTRACT OR GRANT NUMBER: <u>Contract DAAG29-77-C-0048</u>

5. NAME OF INSTITUTION: <u>Massachusetts Institute of Technology</u>

6. AUTHOR(S) OF REPORT: <u>Warren S. Ross</u>

7. LIST OF MANUSCRIPTS SUBMITTED OR PUBLISHED UNDER ARO SPONSOR-
   SHIP DURING THIS PERIOD, INCLUDING JOURNAL REFERENCES:

   None

8. SCIENTIFIC PERSONNEL SUPPORTED BY THIS PROJECT AND DEGREES
   AWARDED DURING THIS REPORTING PERIOD:

   <u>Scientific Personnel</u>

   R. S. Kennedy, Professor

   J. H. Shapiro, Associate Professor

   W. Ross, Research Assistant

Dr Robert S. Kennedy
Massachusetts Institute of Technology
Department of Electrical Engineering
and Computer Science
Cambridge Massachusetts 02139

80 3 7 093

(6) # AN INVESTIGATION OF ATMOSPHERIC OPTICALLY SCATTERED NON-LINE-OF-SIGHT COMMUNICATION LINKS.

U.S. Army Research Office

Contract DAAG29-77-C-0048

(15)

(9) FINAL REPORT,

Sept━━78 ━━ Sept━━79,

(10)

Submitted by: Warren S. Ross

Principal Investigator: Robert S. Kennedy

(11) 5 Jan━━80   (12) 66

(18) ARO   (19) 065.2-A-EL

Massachusetts Institute of Technology

Research Laboratory of Electronics

Cambridge Massachusetts 02139

304050   N

Table of Contents

1.0 Introduction

This report discusses the work performed in the second year of a two year program to investigate short-haul non-line-of-sight optical scatter communication links. The wavelength region considered for this study is the middle ultraviolet (uv) (2000 Å - 3000 Å). This region is attractive for communication purposes because the absence of solar background radiation makes wide-angle receivers practical. Furthermore, the short wavelengths result in significant scatter from molecular atmospheric constituents (Rayleigh scatter), so that the availability of a non-line-of-sight link is extended into clear weather [1].

The goal of the investigation has been to obtain a fundamental understanding of scatter propagation in low visibility atmospheric environments. In particular, the work has focused on the determination of parameters needed for optical communication system design, such as angular spread and multipath time spread.

Since low visibility environments produce significant multiple scattering effects at optical wavelengths, a solely theoretical approach to determining these propagation parameters is extremely complex [2,3]. Hence, a combined experimental/theoretical approach has been followed. In this approach, measurements provide order of magnitude ranges for the propagation parameters, and this information is used to simplify the theoretical propagation equations.

The work in the first year of this program was predominantly experimental [4]. Experiments in Cambridge, Massachusetts, were conducted to obtain representative data about non-line-of- sight propagation of middle ultraviolet light in city environments. Experiments were also conducted to measure angular spreading behavior on a line-of-sight link. Some angular spreading data was obtained in Cambridge, but the majority of the data was obtained during a field trip to Lubec, Maine. In Lubec, the frequency of occurrence of maritime fog made it possible to collect a large amount of low visibility data in a relatively short period of time.

The work during the current year has built on the experimental data base of the first year. Experiments were performed during the current year to supplement this data base. In particular, three

types of experiments were performed:

1) angular spreading experiments: to refine the characterization of angular spreading begun in the first year;

2) visible vs. uv extinction experiments: to measure comparative extinction coefficients in fog for middle uv light (2537 $\overset{O}{A}$) and HeNe laser light (6328 $\overset{O}{A}$).

3) multipath time spread experiments to measure pulse distortion through fog with short pulse uv sources;

These latter experiments will not be reported here, since they were preliminary. We will simply note that for optical thicknesses less than 10 on a 0.43 km path, no multipath spread was observed with a 2 µsec wide pulse.

In addition to these experiments, work is near completion on a modification to existing measuring equipment which will allow automated data collection for future angular spreading measurements [5].

Theoretical work has progressed in a number of areas during the current year. Comparisons have been made between the measured data and predictions from single scatter, diffusion and multiple forward scatter theories. The latter theory, which is on application of results from turbulence theory to a scattering environment [6], is in reasonably good agreement with the measured data. Calculations from various theories have been supplemented by Monte Carlo simulations where necessary.

Some progress has been made in utilizing the experimental data to simplify the linear transport equation, which describes the propagation in a scattering/absorbing medium [7,8]. As initially observed during the first year of this work [4], the amount of light which reaches the receivers at large angles from the line-of-sight direction is relatively insensitive to random spatial variations in the extinction coefficient. This fact has been used to make simplifications to the integral equation for the scattered component of the field.

The experimental and theoretical work conducted during this year are described in more detail in the sections which follow.

2.0 Experiments

This section presents the results of the angular spreading and visible vs uv extinction measurements. The presentation of the data is preceded by a discussion of the methodology used in characterizing the weather conditions, and a description of the measuring equipment utilized.

2.1.0 Measurement of Weather Conditions

To relate theoretical work to the experimental data, it is sufficient to know the scattering coefficient, absorption coefficient and the single scatter phase function resulting from the weather conditions prevailing at the time of the experiments. It is a relatively simple matter to measure the scattering and absorption coefficient, particularly at middle uv wavelengths where the primary absorber is molecular ozone. If ozone concentration is measured at the time of the experiment, then a single extinction measurement will determine tne scattering coefficient.

In practical situations, of course, at any time the scattering coefficient varies randomly as a function of distance along the path. Thus, an extinction measurement involving integration over the entire path is necessary. In general, a path-integrated ozone absorption coefficient would also be necessary. However, if the ozone concentration in a region is relatively stable (e.g., there are no ozone sources nearby), and the path is not too long, a simple point measurement of ozone concentration suffices.

Unfortunately, there is no easy way to measure the single scatter phase function. Measuring the phase function directly, or measuring the particle size distribution - from which the phase function can be determined by Mie calculations - is difficult and time consuming. However, if observations are made of the macroscopic features of the weather conditions (such as qualitative weather type and relative humidity), then published experimental or theoretical phase functions may be used [9, 10].

The procedure used to characterize the atmosphere during our experiments is as follows: First, a qualitative weather type (e.g., fog, snow) is noted, along with any other relevant descriptive information (e.g., high variability in conditions). Second,

temperature and relative humidity are recorded (sometimes after the fact). Third, a point ozone concentration measurement is made at the receiver. Finally, the average path extinction coefficient is determined.

This latter quantity is derived by comparing the power received on a clear day in a 1 milliradian (mr) field of view (FOV) with that received in the same FOV under low visibility conditions. Since a 1 mr FOV will collect predominantly unscattered light, the negative log of the ratio of these two power measurements is the integrated optical thickness, τ:

$$\tau = \int_0^L \alpha(z)\,dz = -\ln \frac{P_{\text{low visibility}}}{P_{\text{clear}}} \qquad (2.1\text{-}1)$$

Here $\alpha(z)$ is the extinction coefficient as a function of z, the distance along the line-of-sight path from source to receiver. L is the pathlength. τ/L is the average extinction coefficient along the path.

2.2 Equipment Description

A variety of source, receiver and filter combinations were used for the different experiments. Tables 2-1 through 2-3 list their specifications. Figure 2-1 shows schematic diagrams of the three receivers. Table 2-4 shows which combinations of equipment were used for each type of experiment.

In addition to the equipment listed in the tables, ozone measurements were made with a Mast Development Company Model 724-5 Ozone Meter.

Table 2-1   Source Specifications

	Germicidal Lamp	He Ne Laser	Lamp
Pulsed or cw	cw	cw	Pulsed
Pulse width	–	–	1-2 μ sec
Repetition rate	–	–	$\frac{1}{15}$/sec
Power output or energy/pulse	1.4 watts	3 mw	≈ 1 joule
Spectral Characteristics	λ = 2537 Å	λ = 6328 Å	Broadband: uv & visible
Source Size	9" x 1/2"	10" x 10"	5" diam.
Exit beam angle	≈ ± 90°	± 0.8 mr	±15°

Table 2-2 Receiver Specifications

	Variable NFOV Receiver	Fixed WFOV Receiver	Variable WFOV Receiver (Honeywell)
Optical front end	Reflecting telescope: - mirror reflectivity = 90% - focal length = 46"	none	none
Aperture	4 1/4" diameter	4 1/2" diameter	1" diameter
FOV	Variable iris: 1-15 mr (full angle)	Controlled by length of pipe on front end; fixed at 17° (full angle)	Controlled by length of pipe on front end; 84° or 22° (full angle)*
Filter	See Table 2-3	Solution of Ni So$_4$ and Cation X, 10% transmission at 2537 Å	Solid Ni So$_4$ + Cation X: 2.3% transmission at 2537 Å, completely solar blind

PMT	- Bialkali cathode
	- QE = 22% at 2537 Å
	    25% at 2650 Å
	    1.2% at 6328 Å
	- Gain = 2.5 x 10^7 @ 1400 MHV
		- RbTe cathode
		- QE = 8.6% at 2537 Å
		- Gain = 2.6 x 10^7 @ 2000 PHV
			Cs Te cathode
			QE = 6.4% at 2537 Å

Post Detection Processing	Photon counting ** or storage oscilloscope	Photon counting **	Photon counting ***

* made smaller by using longer pipe

**Princeton Applied Research Model 1121 Amp/Disc and Model 1112 Counter/processor

***Internal amp/disc and either Model 1112 counter or Fluke Model 1900 A multi-counter

TABLE 2 - 3 NFOV RECEIVER FILTER SPECIFICATIONS

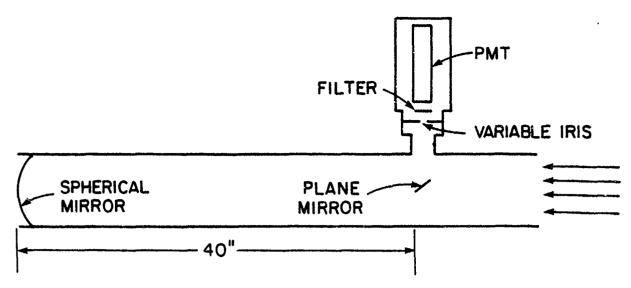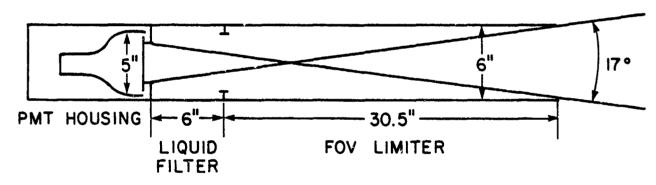|	2537 Å	2650 Å	6328 Å	broadband (Corning 7058 glass)
Transmission	7.7%	6.4%	57%	10% at 2650 Å
Bandwidth (full width half maximum)	81 Å	< 100 Å	107 Å	uv – visible

Fig. 2-1a: Variable NFOV Receiver

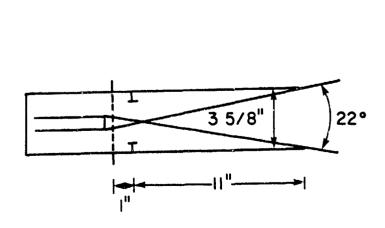Fig. 2-1b: Fixed WFOV Receiver
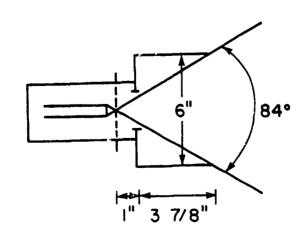

Fig. 2-1c: Honeywell Receiver
(Small FOV)

Fig. 2-1d: Honeywell Receiver
(Large FOV)

Table 2-4 Combinations of Source Receiver, and Filter for Various Experiments

Type of Experiment	Source	Receiver	Filter
Angular Spreading	Germicidal lamp	All three	$\lambda = 2537$ Å
Multipath time spread	Xenon Arc lamp	Variable NFOV	$\lambda = 2650$ Å - broadband
He Ne vs uv extinction	germicidal lamp He Ne laser	Variable NFOV	$\lambda = 2537$ Å $\lambda = 6328$ Å

2.3 Description of Field Trip Experimental Sites

Almost all of the angular spreading data was obtained during field trips to the Maine coast. In the first year of the program experiments were conducted at Lubec, Maine [4]. During the second year, experiments were conducted in the nearby community of Eastport, Maine. This section describes the experimental sites for the Eastport field trip (A description of the Lubec site is given in reference [4].) Section 2.3.1 discusses the prevailing weather conditions in the Eastport area. Section 2.3.2 discusses the experimental link geometry.

2.3.1. Weather conditions in the Eastport Area

The city of Eastport is located in Washington County, Maine, near the mouth of the Bay of Fundy. (See Fig. 2-2). This area ranks third on the east coast in frequency of fog during the year, with an average of 65 days of fog [11]. As can be seen from Fig 2-3, the highest incidence of fog is during the summer months, particularly July [12].

During the first year 18 day field trip to Lubec (July 24 - August 11, 1978), we experienced 7 days of heavy fog. Six of these days were consecutive and during two of them the fog did not lift for the entire 24 hours. We experienced heavy fog during 9 days of the 6 week field trip to Eastport (June 9 - July 20, 1979). The relative frequency of fog in Eastport was lower than in Lubec because the Eastport experimental facilities were located in a cove partially sheltered from the winds which blow the fog inland.

The fog type encountered during these field trips is classified as a stable advection fog [13]. The formation mechanism is typical of coastal maritime fogs, in which warm, moist air condenses over colder sea water and is then blown inland. In general, the fog occuring during the experiments had existed for some time before blowing inland, and hence was a "mature" rather than "evolving" fog [14].

The ozone concentration measured during the Eastport field trip was between 0.5 and 2.0 parts per hundred million (pphm), but the concentration was usually in the 1-2 - 1.8 pphm range. The
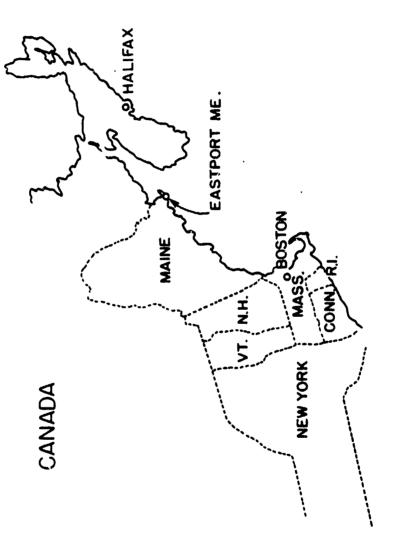
Fig. 2-2: Location of Eastport, Maine
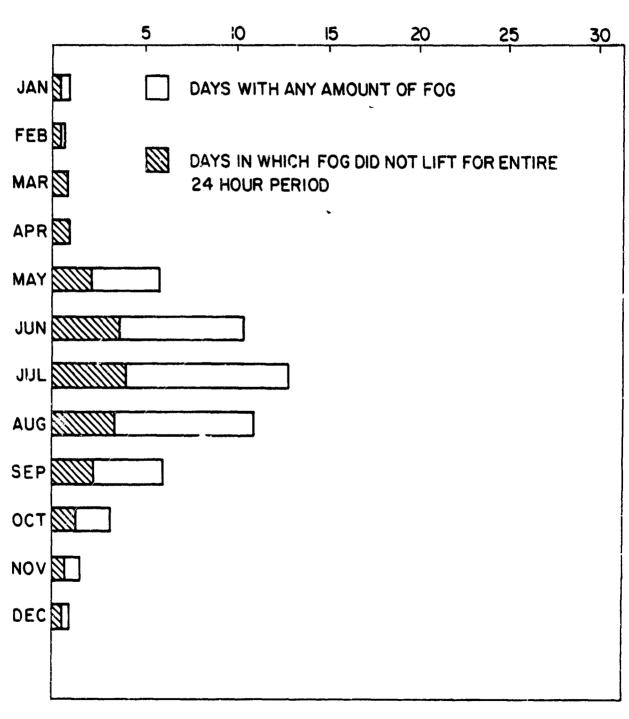
Fig. 2-3: Average Number of Days of
           Heavy Fog
           (Visibility < 0.5 miles)
           for Period Jan. 1960 -
           Dec. 1978

pathlengths used in the field experiments were short enough
(< 1 km) so that ozone concentrations in the above ranges did
not produce significant losses. At a pressure of 1 atmosphere
the ozone absorption coefficient is related to ozone concentra-
tion by [15].

$$\alpha_{O_3}(km^{-1}) = 84.4 \frac{C_{O_3}}{T}, \qquad (2.3-1)$$

where C_{O_3} is the ozone concentration in pphm and T is the ambient
temperature in $^{\circ}K$. Table 2-5 shows ozone absorption coefficients
for the ranges of C_{O_3} encountered in the field trips. Also
included in the table are values of ozone transmission for two
representative pathlengths (0.43 and 0.88 km). The worst case
transmission loss is less than a factor of 2. This is
relatively insignificant by comparison with the scattering losses
of $10^2 - 10^5$ in fog.

Table 2-5 Ozone Absorption Coefficients and Corresponding
Transmission Due to Ozone

C_{O_3} (pphm)

	0.5	1.0	1.5	2.0
$\alpha_{O_3}(km^{-1})$	0.15	0.29	0.44	0.58
$T = e^{-0.43\,\alpha_{O_3}}$	0.94	0.88	0.83	0.78
$T = e^{-0.88\,\alpha_{O_3}}$	0.87	0.77	0.68	0.60

2.3.2 Eastport Link Geometry

A detailed view of the two Eastport sites is shown in Fig 2-4 and the topography of the main propagation link (at the Washington County Vocational Technical Institute's Marine Center) is shown in Fig 2-5. The topography of the Eastport airport (site #2) is, of course, flat, with a rough asphalt surface. For the experiments conducted at the airport site, both the source and receiver were approximately 5 feet off the ground. The facilities at the Vocational Institute allowed for a long path of 0.43 km. Two shorter paths were also established by mounting sources on telephone poles closer to the receiver location at the end of the dock. The two short path distances are .22 km and .32 km. Experiments at the airport were conducted with a fixed source and the portable Honeywell receiver.   Pathlengths varied from about 1.2 km to .88 km.

2.4 Angular Spreading Experiments

Although a significant amount of fog angular spreading data was obtained during the first year of this program, most of it was limited to a relatively narrow range of optical thickness ($5 < \tau < 9$). Thus one important goal of this year's experiments was to explore the regions $\tau < 5$ and $\tau > 9$.

Another major goal was to verify a number of basic features of the fog angular spectrum that had been identified after analyzing the Lubec data. Briefly, these features are [4]:

1) There is a measureable unscattered signal component for $\tau < 9$;

2) This unscattered component falls below the scattered component for $\tau > 10$ and a uniform angular spectrum result (at least for the angular region $|\theta| < 12$ mr

3) For $\tau > 5$, the 10 dB halfwidth of the angular spectrum is between 5 and 10 mr. The spectrum tends to broaden as τ increases;

4) For off-axis angles, the received signal is relatively insensitive to spatial variations in the extinction coefficient, while the on-axis (or unscattered) signal is quite sensitive to these variations
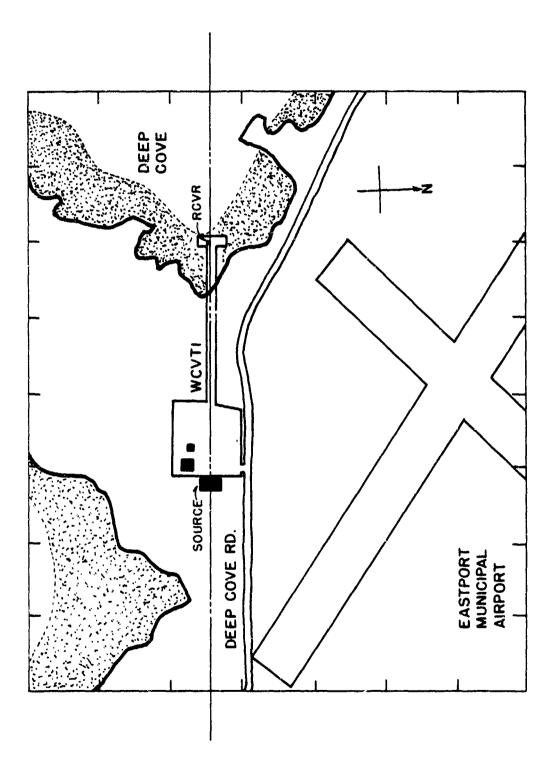
Fig. 2-4: Overhead View of 2 Eastport Sites (WCVTI and Airport)
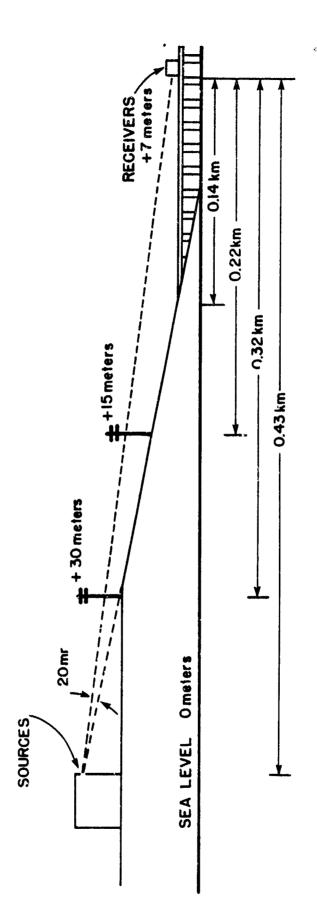
Fig. 2-5: Side View of WCVTI
Propagation Link

5)   The relatively uniform portion of the angular spectrum
      extends pver a considerable range, at least as far out
      as 25°.

Figs. 3-1 and 3-2 of refererce [4] are pictorial representations
of these features.

Finally, it was our goal to determine to what extent the
above features were influenced by absolute pathlength. Most of
the measurements to date had been at a single pathlength; optical
thickness, which is a normalized pathlength, was used to
characterize the path. We wanted to find out how the measured
results for a given optical thickness would be affected by different
pathlengths.

Although the fog was never thick enough during the Eastport
field trip to get data for $\tau > 9$, most of the other goals were
achieved: significant data was obtained for $\tau < 5$; characteristics
1), 3) and 4) listed above were repeatedly observed in the region
$5 < \tau < 9$ (although some of the angular spectrum 10 dB half widths
were less than 5 mr); some multiple pathlength data were obtained.
In the rest of this section, the data are presented and discussed.

Table 2.6 is a summary of the small angle signal versus
collecting FOV data, and Table 2-7 summarizes the angular scan data.
Fig 2-6 shows a comparison of signal collected by a narrow FOV
(1 mr full angle) receiver with that collected by a wide FOV (84°
full angle) receiver.

In order to see how the angular spectrum broadens as τ
increases, the small angle signal vs. FOV data has been plotted
with τ as a parameter. The curves are drawn throuyn the mean
values of the data of each FOV. (See Fig. 2-7). Observe that most
of the data are consistent with the conclusion that the angular
spectrum broadens as the optical thickness increases.

Table 2-6

SUMMARY OF UV SIGNAL VS. FOV DATA: EASTPORT, 1979 ✝

Date	Time	Optical Thickness	Multiplication of Mean Signal Level 5 mr	10 mr	15 mr
6/23	4:10 am	3.1-4.4	1.7-2.1	2.4-3.0	2.8-3.6
	4:00	2.8	2.1	2.6	2.9
	4:20	1.8-2.1	1.8-2.4	1.8-2.4	1.9-2.5
	4:25	3.4-3.7	1.8-2.5	2.1-2.9	2.1-2.9
	4:20	5.9(?)	1.9	1.8	2.7-3.5
	4:30	4.0	2.4	3.5	4.2
	4:33	4.0	2.0	3.0	3.4
	4:36-40	4.3	2.0	3.7	3.9
	5:15	3.9	2.3	3.0	3.5
	5:10	3.4	2.1	2.8	3.1
	5:20	3.7	2.5	2.8	3.1
	5:20	4.0	2.1	3.2	3.7
	10:20 pm	6.3	2.8	4.9	7.6
	11:40	5.6-6.1	2.4-3.9	3.4-5.6	3.6-5.9
	11:45	6.2	3.1	5.2	5.9
7/1	12:20 am	***			
	12:23	5.2	2.4	4.0	4.9
	12:30	4.9	2.1	3.5	4.0
	3:30	4.8	2.9	5.6	6.2
	3:40	4.4-4.7	2.8-4.1	5.6-8.2	5.5-8.0
	3:50	4.6	3.7	5.8	7.3
	11:10-15 pm	3.3	2.8	3.9	4.5
7/2	5:43 am	6.5	7.7	12.5	14.8
	5:45-48	6.3	3.8	8.3	11.7
	10:13 pm	4.3	1.8	3.2	3.9
	11:50	***			
	11:53	6.4	2.3	3.3	4.9
	11:55	6.8	3.0	4.8	5.8
7/3	12:00 am	7.1	2.7	4.0	6.2
	1:35	***			
7/16	3:50 am	4.0-4.4	1.3-1.8	2.1-3.0	---

***Data obtained but weather too variable to make
    a reliable estimate of optical thickness.

✝ Pathlength = 0.43 km, FOV for unscattered measurement = 1.0 mr.

Table 2-7

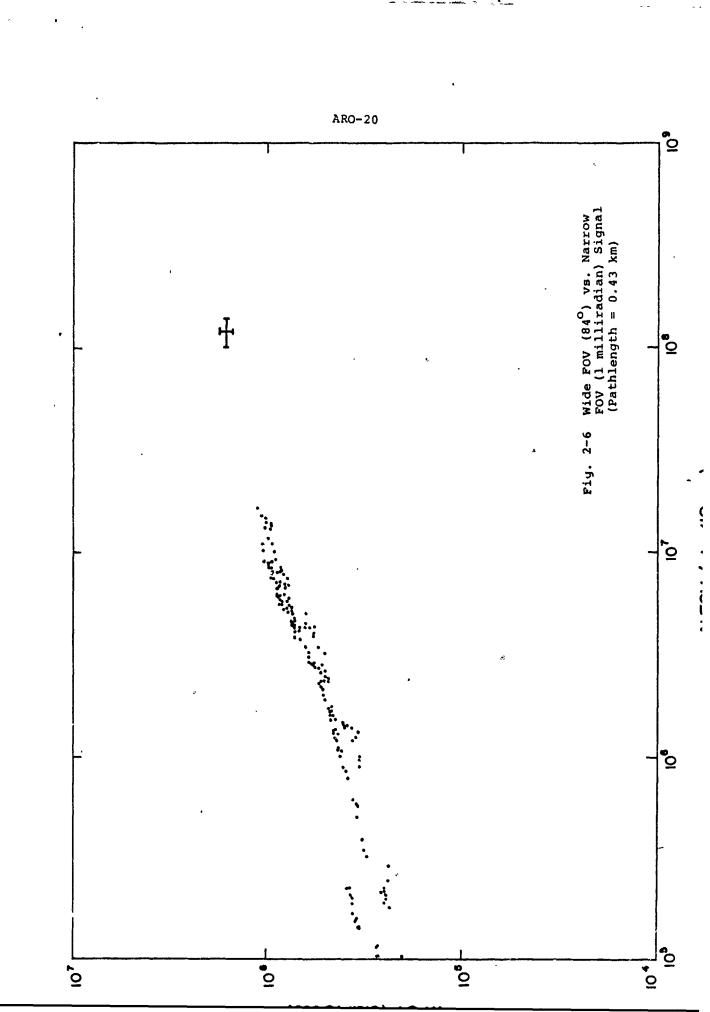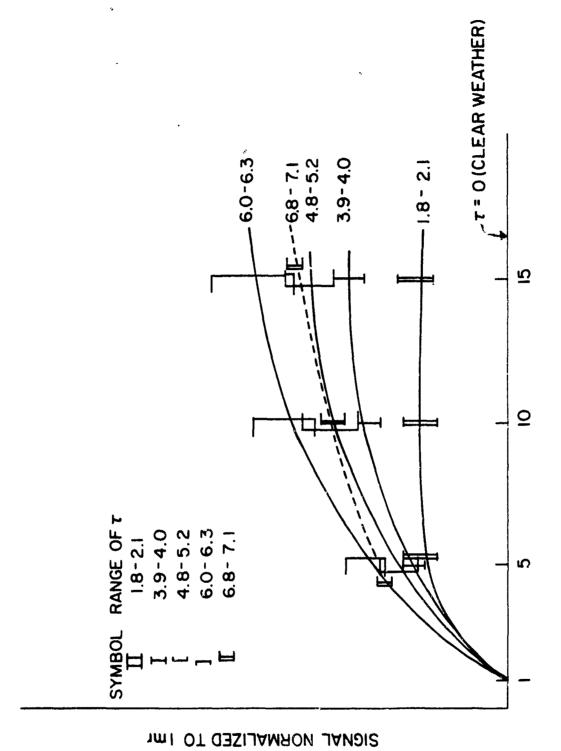SUMMARY OF ANGULAR SPECTRUM DATA: EASTPORT, 1979 [*]

Date	Time	Optical Thickness	Type	10 dB Half Width
6/23	10:25 pm	5.5-5.9	az	4 mr
	10:50	8.4-8.7	el	4-6 mr
	11:50	5.3	el	3 mr
6/24	12:00 am	5.1	el	2.5 mr
6/25	10:30 pm	0	az	1 mr
	11:10	0	el	1.25 mr
7/1	3:52 am	4.4-5.1	el	5-7 mr
	4:15	***		
7/3	12:07 am	7.1	az	4.5-5.0 mr
	12:30	6.3	el	7 mr
	12:45	5.1-6.0	az (5 mr FOV) [**]	---
	1:25	5.0-6.0	az (5 mr FOV)	---
7/12	1:30 am	***	az (5 mr FOV)	
	1:50	6.0-6.5	az (5 mr FOV)	---
	3:20	7.0-8.0	el (5 mr FOV)	
	3:50	8.3	el	9 mr

*** Data obtained, but weather too variable to make
a reliable estimate of optical thickness.

[**] Scan was done with a 5 mr FOV instead of a 1 mr FOV

[*] Pathlength = 0.43 km

Fig. 2-6 Wide FOV (84°) vs. Narrow FOV (1 milliradian) Signal (Pathlength = 0.43 km)

Fig. 2-7: Signal vs. FOV Curves for Different Ranges of τ.

The inversion of the curves for $6.0 < \tau < 6.3$ and $6.8 < \tau < 7.1$ appears to violate this conclusion, but the large error bars on the $6.0 < \tau < 6.3$ data overlap (or nearly overlap) the error bars for the $6.8 < \tau < 7.1$ data. Indeed, if the measurements on 7/2/79 (5:45-48 am) are not included in the data for the latter range, the two curves are quite close together. There are other examples in Table 2-6 of data that are not consistent with this conclusion, but the majority of the data tend to support it.

The curves in Fig. 2-7 only show signal level relative to the 1 mr value in any optical thickness region. Of course, the signal levels for the larger ranges of optical thickness are below those for the smaller ones. Figures 2-8 through 2-10 show this optical thickness dependence explicitly, with FOV as a parameter (The 5 mr, 10 mr and 15 mr curves are shown in separate figures for clarity.) Included in these figures is the corresponding curve for an 84° full angle FOV, obtained from Fig. 2-6.
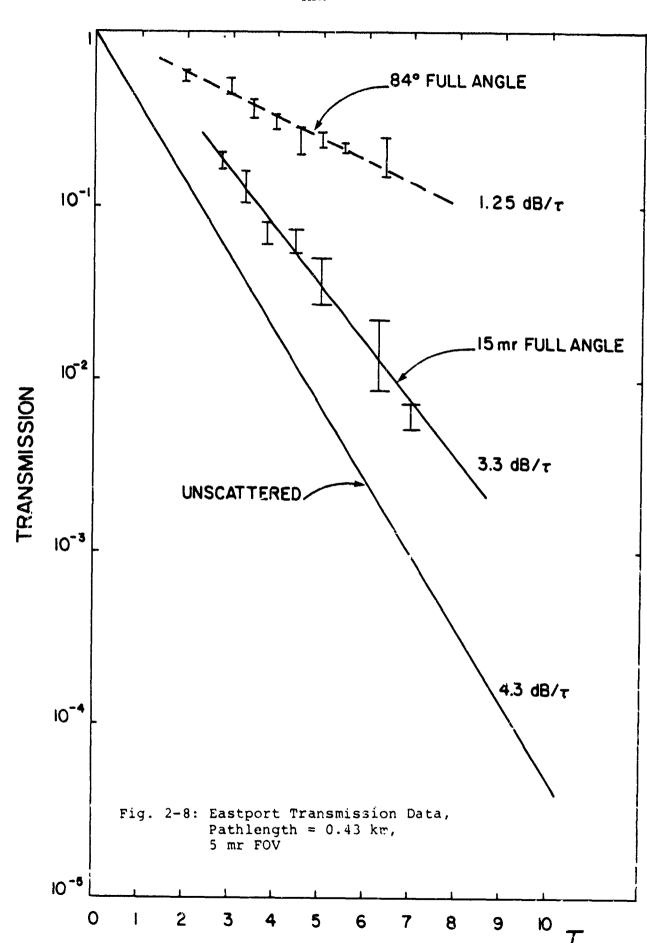
As can be seen from the figures, the data points for any single FOV very nearly lie on a straight line. The slope of this line is dependent upon the FOV, ranging from 3.8 dB transmission loss per optical thickness (for FOV = 5 mr) to 1.25 dB per optical thickness (for FOV = 84°). Thus the data suggest a general exponential extinction law valid for a receiver processing both the scattered and the unscattered signal components:
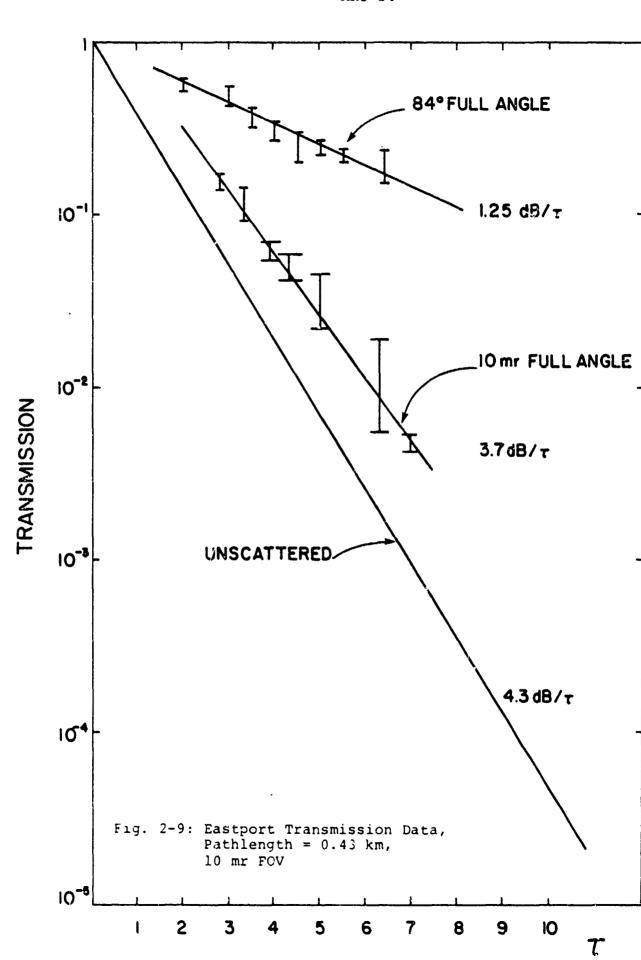
$$P_r \sim P_T \, e^{-f(FOV)\tau} \qquad\qquad (2.4\text{-}1)$$

where $f(FOV)$ is always less than 1 and is a monotonically decreasing function of the FOV.

We defer any further discussion of the function $f(FOV)$ until after the multiple pathlength data is presented. Some understanding of the pathlength dependence of the angular spreading is needed in order to use data taken over different pathlengths to compute a universal function $f(FOV)$.

Multiple path transmission experiments were conducted at the Eastport airport, with the source location fixed and the receiver
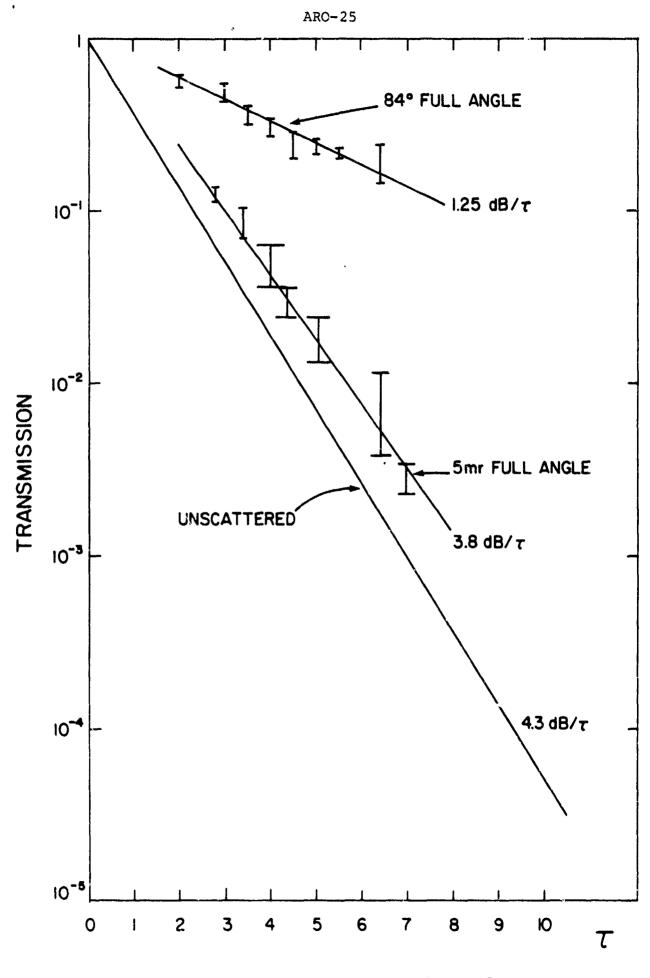
Fig. 2-8: Eastport Transmission Data,
        Pathlength = 0.43 km,
        5 mr FOV

Fig. 2-9: Eastport Transmission Data,
Pathlength = 0.43 km,
10 mr FOV

Fig. 2-10: Eastport Transmission Data,
Pathlength = 0.43 km,

location variable. The portable Honeywell sensor was used with both the 22° and 84° field of view. Measurements were made with both source and receivers mounted about 5 feet from the ground.

Time limitations due to weather variability made it impossible to measure optical thickness directly during these experiments. (Aiming to within a milliradian requires a few minutes of time under the best of circumstances). Thus, the values of τ (and hence α, the extinction coefficient) were inferred from the 84° FOV trans- mission data by comparing the data at a pathlength of 0.47 km with the narrow versus wide FOV data in Fig 2-6. (The comparison here is not perfect, since the latter data were taken over a 0.43 km path with somewhat different boundary conditions. (See Fig 2-5b.) However, the 0.04 km difference is not very significant, and in both sets of boundary conditions, most of the scattered signal will come from the upper hemispheres.)

Table 2-8 presents the results of the multiple path transmission experiments for two fog thicknesses, $\alpha = 11.0$ km^{-1} and $\alpha = 15.2$ km^{-1}. In Figures 2-11 and 2-12, these data are compared with data taken at the same fields of view but with a fixed pathlength. For the 84° FOV, the fixed pathlength measurements were made on the 0.43 km path in Eastport. For the 22° FOV, the fixed pathlength measurements were made on the 0.30 km path over water at Lubec.

The data in Figures 2-11 and 2-12 are somewhat equivocal with respect to determining the sensitivity of the result to pathlength. If the $\tau = 9.7$ data points can be ignored, then the remaining multiple pathlength data lie fairly close to the fixed pathlength line. However, there are not enough data at the larger optical thicknesses to justify calling the $\tau = 9.7$ point anomalous. In fact, if the $\tau = 13.4$ data points are ignored, then a very different conclusion results.

There is further evidence of the relative pathlength insensitivity of our results, however. During the Lubec field trip in 1978, narrow versus wide FOV measurements were made with a 17° full angle FOV, at both 0.30 km and 1.6 km. (See Figures A-18 and A-19 of reference [4].) These two sets of data are plotted together in Fig. 2-13. Although most of the 0.3 km data are for $\tau < 6$ and most of the 1.6 km data are for $\tau > 6$, it is clear from the figure that both
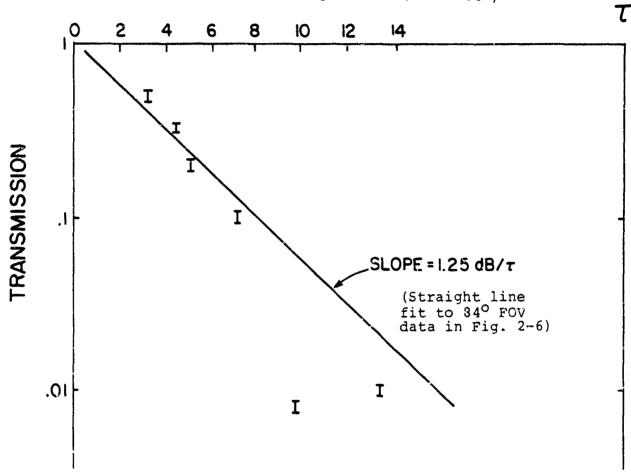
TABLE 2-8a. MULTIPLE PATH TRANSMISSION LOSS DATA
$$(\alpha = 11.0 \ km^{-1})$$

Distance (km)	τ	$\mathcal{L}_{84}o$ (dB)	$\mathcal{L}_{22}o$ (dB)	$\mathcal{L}_{ext}$ (dB)
.29	3.2	3	5	14
.47	5.1	7	10	22
.88	9.7	21	23	42

TABLE 2-8b. MULTIPLE PATH TRANSMISSION LOSS DATA
$$(\alpha = 15.2 \ km^{-1})$$

Distance (km)	τ	$\mathcal{L}_{84}o$ (dB)	$\mathcal{L}_{22}o$ (dB)	$\mathcal{L}_{ext}$ (dB)
.29	4.4	5	7	19
.47	7.1	10	13	31
.88	13.4	20	24	58

Fig. 2-11 Comparison of Multiple Path-
length Data with Straight
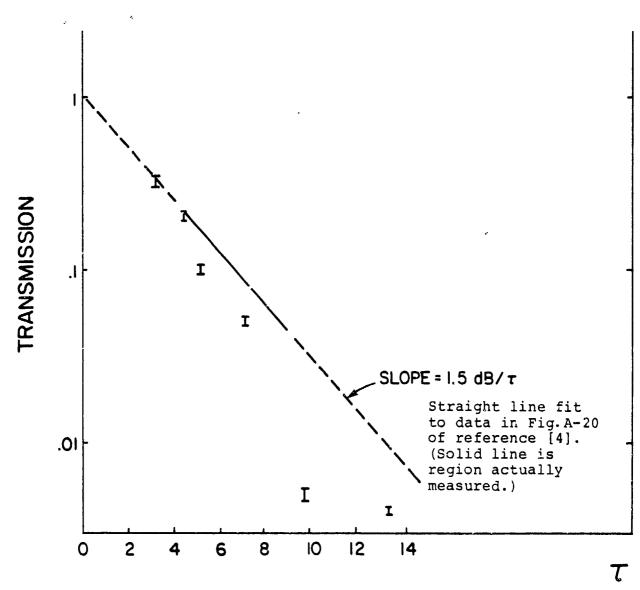Line Fit to Fixed Path-
length Data (FOV = 84°)

Fig. 2-12: Comparison of Multiple
Pathlength Data with
Straight Line Fit to Fixed
Pathlength Data (FOV = 22°)

groups of data fall along a straight line, whose slope is approximately 2.5 dB per optical thickness.

Fig. 2-13, combined with Figs. 2-11 and 2-12, is strong evidence that, at least over the pathlength ranges covered in our experiments, the character of the transmission curve is not highly sensitive to absolute pathlength. Table 2-9 summarizes the available data for transmission vs. FOV in terms of the slope of the transmission curve. The corresponding value of f(FOV), the coefficient in the exponential transmission law Eq. 2.4-1, is shown for each FOV.
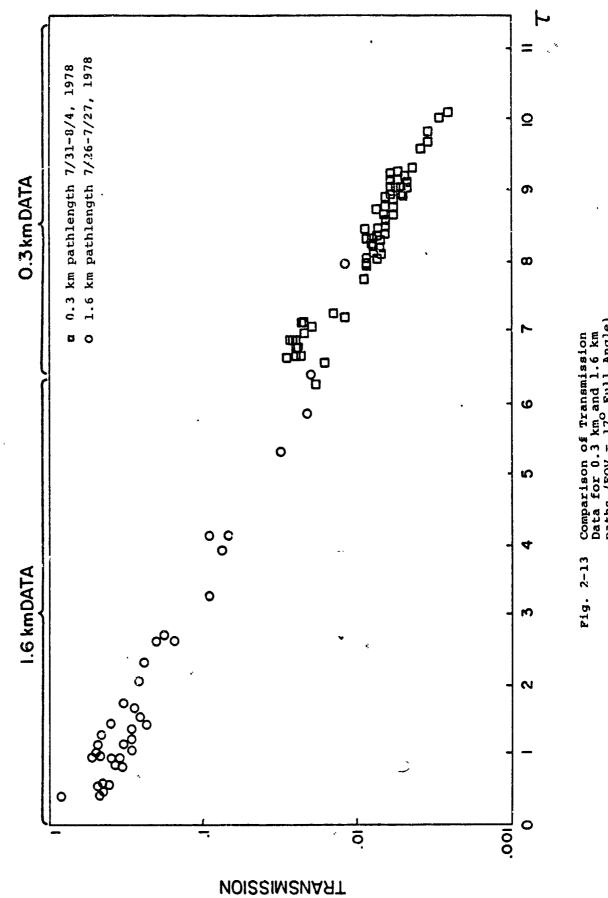
Figure 2-14 is a plot of f(FOV) versus FOV. (Note that the 1 mr point is assumed to be unscattered signal so that f(FOV) = 1). With the limited data available, it is difficult to determine an analytical function for f(FOV) with any great precision. However, the functions appear to be roughly logorithmic with FOV. Assuming this to be the case, our empirical formula for f(FOV) (FOV in mr) is given by
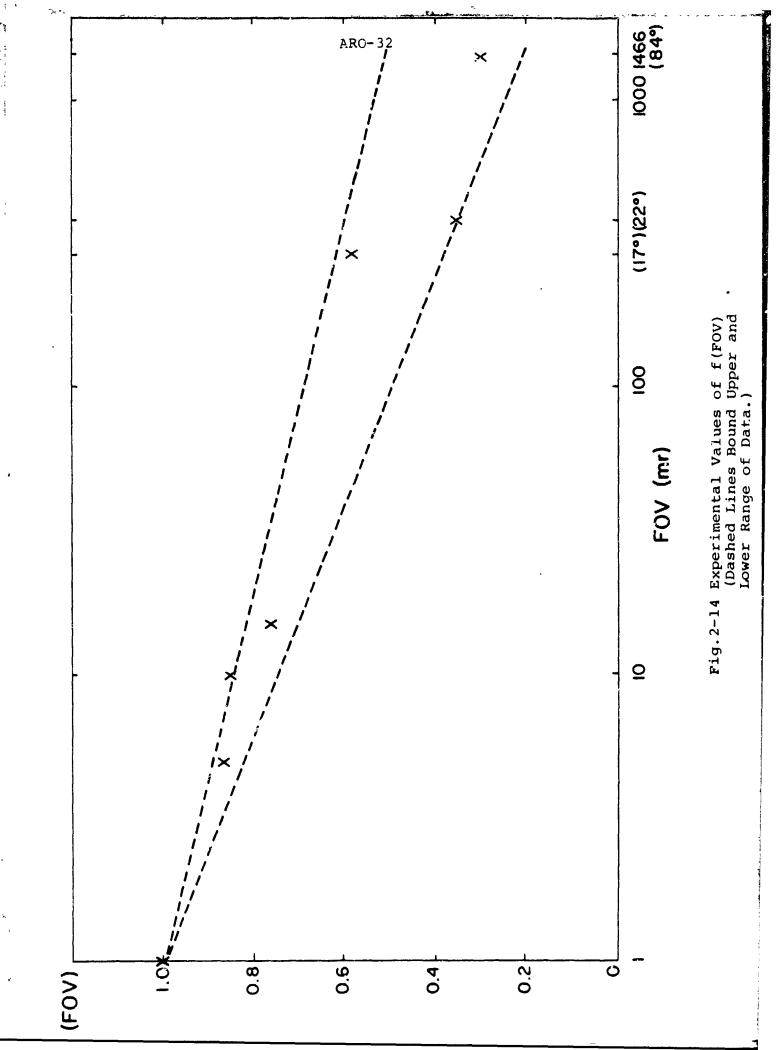
$$f(FOV) = 1 - k \ln(FOV) \quad (1 < FOV < 1500 \text{ mr}), \quad (2.4-2)$$

where K is in the range 0.069 - 0.11.

Table 2-9 Summary of Transmission Data

FOV	Pathlength (km)	Slope of Transmission Curve	f(FOV)
5 mr	0.43	-3.8 dB/τ	.87
10 mr	0.43	-3.7 dB/τ	.85
15 mr	0.43	-3.3 dB/τ	.76
17°	0.30	-2.5 dB/τ	.58
17°	1.6	-2.5 dB/τ	.58
22^0	0.30	-1.5 dB/τ	.35
84°	0.43	-1.25 dB/τ	.29

Fig. 2-13 Comparison of Transmission
Data for 0.3 km and 1.6 km
paths (FOV = 17° Full Angle)

Fig. 2-14 Experimental Values of f(FOV)
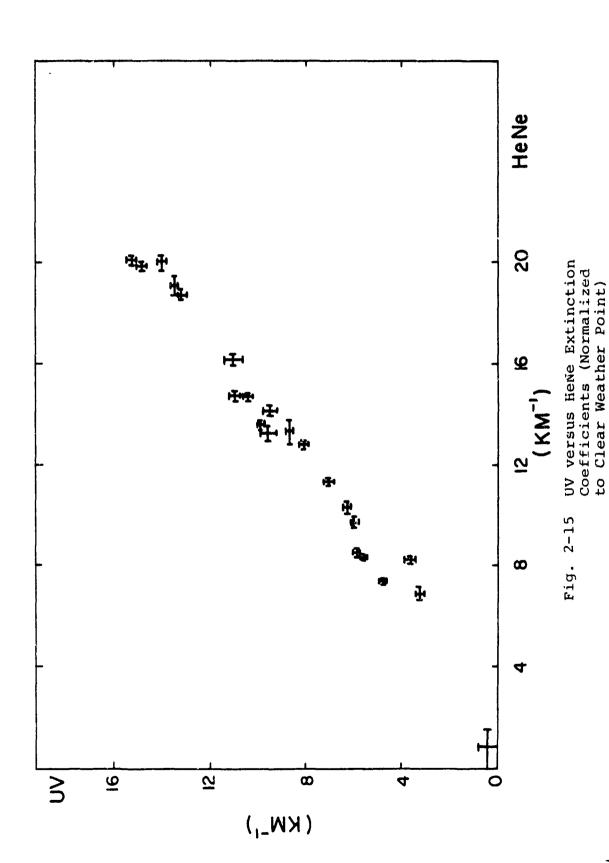(Dashed Lines Bound Upper and
Lower Range of Data.)

2.5 Relation of UV to Visible Extinction

Of crucial importance to assessing the expected performance of a field operated communication system is the ability to make relatively simple optical thickness measurements. In the visible portion of the spectrum, crude estimates of optical thickness can be obtained from observations of visual range. However, to use such observations for a uv system, it is necessary to relate the extinction coefficients for uv and visible light. To this end, we have made extensive measurements of middle uv (2537 $\overset{o}{A}$) versus HeNe laser (6328 $\overset{o}{A}$) extinction coefficients in fog. For these experiments, the two sources were located at a distance of 0.43 km from the receiver and 0.3 meters apart. A single narrow FOV receiver was sequentially aimed at one or the other of the two sources, each of which was viewed with a narrow band filter centered at the appropriate wavelength. (Once clear weather acquisition of one or the other of the sources was obtained, the other source could be acquired easily, even in heavy fog. Relatively little re-aiming was required and could usually be accomplished by peaking the signal from one or the other sources.)

Fig. 2-15 is a plot of measured uv versus HeNe laser extinction coefficients. Observe that for α_{HeNe} greater than 8 km^{-1}, the two coefficients are roughly linearly related. Of course, since the two must both be very close to zero in clear weather (ignoring ozone absorption in the uv), this behavior cannot continue for smaller values of α_{HeNe}. We do not have any data in the region $\alpha_{HeNe} < 8$. (This region corresponds to the onset of fog which usually occurs rapidly enough that it is very difficult to make reliable measurements). In the region $8 < \alpha_{HeNe} < 20$, a least squares fit to the data in Fig 2-15 is

$$\alpha_{uv} = -2.06 + 0.83 \; \alpha_{HeNe} \qquad (2.5-1)$$

The slope of 0.83 relating the two coefficients is somewhat disturbing in light of the published measurements of Baum and Dunkelman [2 8] and the theoretical predictions of Shettle [29]. Shettle predicts that the fog extinction coefficient is insensitive to wavelength in the region from the middle uv through the visible. Baum and Dunkelman show the coefficient to be slightly decreasing as wavelength increases, although their measurements may be biased toward
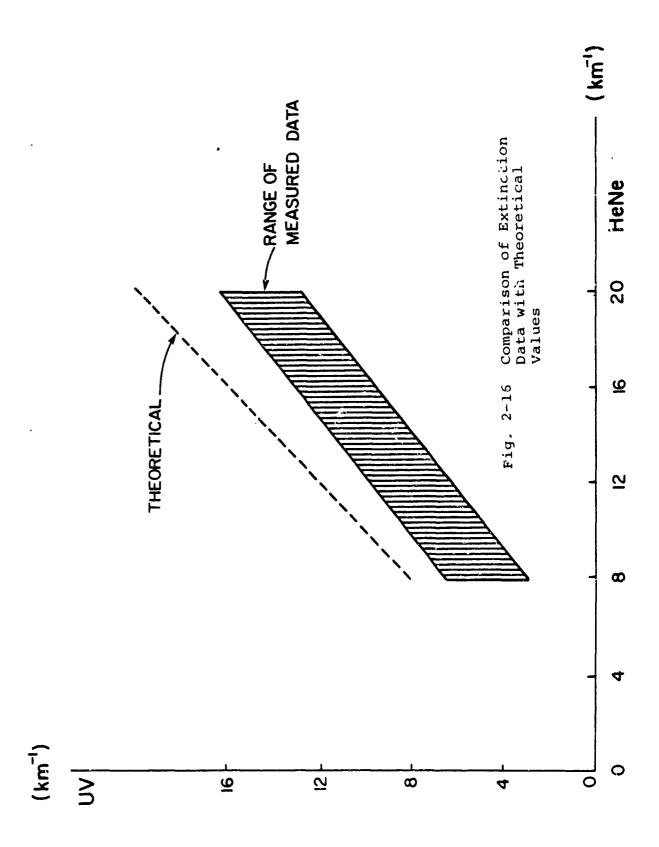
Fig. 2-15 UV versus HeNe Extinction
Coefficients (Normalized
to Clear Weather Point)

higher uv coefficients due to uncertainties about ozone concentrations. In both cases, the slope of the α_{uv} vs. α_{HeNe} curve is greater than or equal to one, compared to a slope of 0.83 for our measurements.

Note, however, that the error bars on the clear weather point (with respect to which all the data are plotted) are rather large, spanning a distance of 1.6 km^{-1} for α_{HeNe} and ± 0.7 km^{-1} for α_{HeNe} around the straight line fit. Hence, the α_{uv} vs α_{HeNe} curve may be shifted to the left by 2.3 km^{-1} or down by 1.7 km^{-1}. The data in Fig. 2-15 are thus bounded by the two lines.

$$\alpha_{uv} = -0.15 + 0.83 \; \alpha_{HeNe}$$

$$\alpha_{uv} = -3.76 + 0.83 \; \alpha_{HeNe} \tag{2.5-2}$$

This region is shown in Fig. 2-16 along with the theoretical curve ($\alpha_{HeNe} = \alpha_{uv}$). A straight line with a slope of one is certainly possible within the range of the data indicated. However, there is still a small absolute shift toward smaller values of α uv.

The difference between our measured relationship and Shettle's predicted one may reflect the difference between the actual particle size distribution we encountered and his specific assumptions about the particle size distribution. His curves show that there is some wavelength beyond which the fog extinction coefficients increase slightly with increasing wavelength. (For his choice of particle sizes, this critical wavelength is above 1 μm.) This critical wavelength is most probably the one at which the wavelength becomes comparable to the mode radius of the particle size distribution. If the distribution were shifted somewhat toward shorter values of radii, the extinction coefficients might exhibit the observed increase of 1-2 km^{-1} at the high end of the visible spectrum.

Fig. 2-16 Comparison of Extinction
Data with Theoretical
Values

3.0 Comparison with Existing Propagation Theories

In this section, a discussion of existing channel propagation theories is presented. These theories include the extremes of single scatter and diffusion, as well as multiple forward scatter theory [6, 16, 17]. Comparisons between the predictions of these theories and the experimental data presented in Section 2.0 is the primary goal of this section. The comparisons give a clear idea of where the data lies in the spectrum between diffusion and single scatter, and of what still needs to be understood.

3.1 Results from Propagation Theories

In this section, the relevant theoretical expressions are presented, with a brief discussion of the appropriate context of each of the theories.

3.1.1. Single Scatter Theory

Single scatter theory adequately describes propagation when the probability is very small that a photon will be scattered more than once between transmitter and receiver. An alternative viewpoint for larger optical thicknesses is that single scattering theory describes the first scattering order of the multiply scattered field.

The point of departure for the present discussion is the theory presented in reference [18], based on the work in reference [1]. The authors present expressions for received intensity as a function of time for an impulsive source. The derivation is carried out in prolate spheroidal coordinates, with the transmitter and receiver located at the foci of an ellipsoid. See Fig. 3-1. This approach is well suited to the problem because of the property that the sum of the distances between the foci and any point on the ellipsoid is a
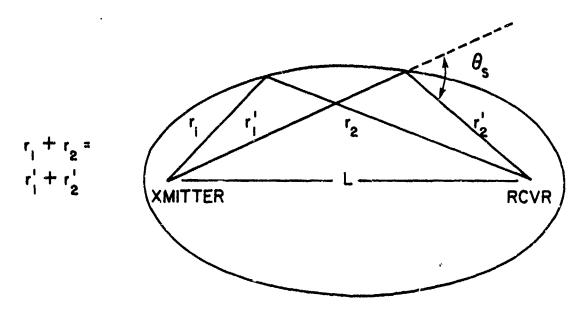
$$r_1 + r_2 = r_1' + r_2'$$

Fig. 3-1 Single Scatter Geometry

constant. Hence, ellipsoids are equitemporal surfaces; i.e., computing the total single scattered radiation reaching the receiver at any one time only involves an integration over this surface.

The total received energy density integrated over the entire scattering volume is given by

$$E_r = \int_V \frac{E_t \alpha_s}{4\pi\Omega_t} \; \frac{\exp\,[-\alpha(r_t + r_r)]}{r_t^2 r_r^2} \; p(\theta_s)\,dV \;, \qquad (3\text{-}1)$$

where

E_t = transmitter energy in [joules];

E_r = received scattered energy density, in [joules/m^2];

α = extinction coefficient;

α_s = scattering coefficient;

r_t = distance from transmitter to scattering event;

r_r = distance from scattering event to receiver;

Ω_t = transmitter solid angle;

θ_s = scattering angle at the scattering event;

$p(\theta_s)$ = single scatter phase function;

V = scattering volume as determined by the transmitter beam pattern.

The phase function is a composite of two functions:

$$p_{Rayleigh}(\theta_s) = \frac{3}{4}(1 + \cos^2 \theta_s) , \qquad (3-2)$$

$$p_{Mie}(\theta_s) = \frac{1 - g^2}{(1 + g^2 - 2g \cos \theta_s)^{1.5}} . \qquad (3-3)$$

Thus,

$$p_{total}(\theta_s) = \frac{\alpha_{s_{Mie}} p_{Mie}(\theta_s) + \alpha_{s_{Rayleigh}} p_{Rayleigh}(\theta_s)}{\alpha_{s_{Mie}} + \alpha_{s_{Rayleigh}}} , \qquad (3-4)$$

where $\alpha_s = \alpha_{s_{Mie}} + \alpha_{s_{Rayleigh}}$. The Mie phase function is the commonly used Henyey-Greenstein phase function [18]. Here, g is the average cosine of the aerosol scattering function:

$$g = 2\pi \int_0^\pi \cos\theta_s p_{Mie}(\theta_s) \sin\theta_s ds. \qquad (3-5)$$

The single scatter theory as presented in reference [18] assumes a pulsed source. For comparison of the single scatter results with cw source measurements, the received pulse is simply integrated over all time.

3.1.2. Diffusion Theory

Diffusion theory is applicable in a very highly multiple scattering environment, which is the opposite extreme to that of single scatter. The precise point at which atmospheric conditions are such that diffusion theory is applicable to uv propagation is still an open question. However, an estimate can be made as follows: Kennedy [19] has shown that for isotropic scatter with large single scatter albedo (>0.9), diffusion theory gives essentially the same results as the exact transport equation solution, for optical thicknesses between 1 and 100. Bucher [20] has shown that many isotropic scatter results can be applied to non-isotropic scatter situations as long as the diffusion thickness, τ_d, is equivalent in the two cases and is greater than 3. Here

$$\tau_d = \tau (1 - g) , \tag{3-6}$$

where τ is the optical thickness of the medium and g is the single scatter phase function's average cosine. (See Eq. (3-5).) For an average cosine of g=0.85 (typical of middle uv phase functions in fog), this criterion implies an optical thickness greater than 20.

The diffusion theory expressions relevant to the present discussion can be derived by introducing Fick's diffusion law into the transport equation [19,21]. With a cw isotropic point source embedded in an infinite medium, the received irradiance is given by [19]

$$\Phi(L,\theta) = P_T \cos\theta \; \frac{\exp\;(-KL)}{(4\pi)^2 DL} \; [1 + \frac{3D(1 + KL)}{L} \cos\theta], \qquad (3\text{-}7)$$

where

P_T=transmitter power;

c=speed of light;

L=source to receiver distance along the optical axis;

θ =angle of arrival of the incoming light relative to the

optical axis;

$D=1/[3(\alpha -g\alpha_s)]$;

α =extinction coefficient;

α_s=scattering coefficient;

$K=[(\alpha -\alpha_s)/D]^{1/2}$.

Eq. (3-7) is the diffusion expression for a cw source. For a pulsed source, the time dependent solution to the diffusion regime transport equation yields the following expressions for the full width to half maximum (FWHM) spread of the received pulse [19]:

$$\text{FWHM} = \begin{cases} \dfrac{1.7L^2}{4cD} & \alpha_a = 0 \\[2em] (0.37 - 1.7)\,\dfrac{L^2}{4cD} & \dfrac{\alpha_a L^2}{4D} \leq 1.5 \\[2em] 1.67\,\dfrac{(L^2/4D)^{1/4}}{c\,(\alpha_a)^{3/4}} & \dfrac{\alpha_a L^2}{4D} > 1.5 \end{cases} \qquad , \qquad (3\text{-}8)$$

where $\alpha_a = \alpha - \alpha_s$ is the absorption coefficient and all other quantities are as defined following Eq. (3-7).

In subsection 3.2.3, the diffusion theory FWHM pulse spread is compared with the single scatter and multiple forward scatter results.

3.1.3 Multiple Forward Scatter Theory

The narrow angle forward scattering approximation has been receiving increasing attention in atmospheric scattering contexts [6,16,17,22] Although different authors introduce it in a variety of ways, the approximation essentially consists of replacing the actual single scatter phase function with one that has only a very narrow forward scatter component. All the backscattered and wide-angle scattered light is assumed to be completely lost to the receiver, and hence is lumped into an absorption term.

The motivation for using such an approximation stems from the persistent narrowness of measured angular spectra and lack of significant multipath spreading for optical thicknesses less than 20 [17,23,24]. Bucher has observed [25] that the dominance of the multiple forward scattered component in the received field may explain the better than expected performance of many simple

laser communication systems in bad weather.

The specific formulation of the multiple forward scatter theory that will be used here is the Extended Huygens-Fresnel Principle developed by Shapiro [6] in analogy with results from turbulence theory [26]. The geometry is
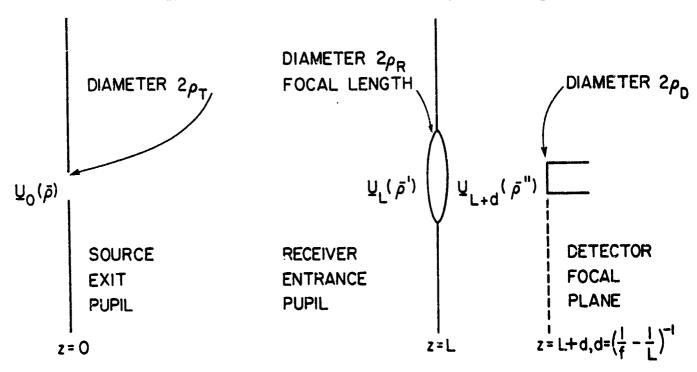
DIAMETER $2\rho_T$

DIAMETER $2\rho_R$
FOCAL LENGTH

DIAMETER $2\rho_D$

$\underline{U}_0(\bar\rho)$

$\underline{U}_L(\bar\rho')$ $\underline{U}_{L+d}(\bar\rho'')$

SOURCE
EXIT
PUPIL

RECEIVER
ENTRANCE
PUPIL

DETECTOR
FOCAL
PLANE

$z=0$

$z=L$

$z=L+d, d=\left(\frac{1}{f}-\frac{1}{L}\right)^{-1}$

Fig. 3-2 Geometry for Extended Huygens- Fresnel Principle

shown in Fig. 3-2.

The discussion in reference [6] is exclusively in terms of a laser source. Here the basic theoretical result is applied to a spatially incoherent source such as the mercury vapor lamp used in the uv experiments. For the conditions encountered in the experiments, the resulting expression for $\langle P_d \rangle$, the average power detected at the focal plane, is

$$\langle P_d \rangle = \frac{\langle P_R \rangle (\text{FOV})^2}{\left[2\left(\frac{\lambda}{\pi\rho_0}\right)^2 + (\text{FOV})^2\right]} \qquad (3-9)$$

where $\langle P_R \rangle$ is the average power arriving at the receiver entrance pupil,

where $\langle \Gamma_R \rangle$ is the average power arriving at the receiver entrance pupil,

$$\langle P_R \rangle = \frac{P_T}{L^2} \, \pi \, \rho_R{}^2 \, e^{-\alpha_a L}, \qquad (3\text{-}10)$$

FOV is the full angle FOV of the receiver, and

$$\rho_0 = (\alpha_s L \theta_0 k^2 / 3)^{-1/2} \qquad (3\text{-}11)$$

is the channel coherence length. θ_0 is the width of the narrow forward peak in the phase function (See Fig. 3-3.), and $k = 2\pi/\lambda$.

Multipath time spread in the multiple forward scatter regime is given by [27]:

$$\text{rms width} = \frac{L}{C} \left[\frac{0.30}{\Theta} [1 + 2.25\Theta)^{1.5} - 1] - 1 \right] \qquad (3\text{-}12)$$

Here c is the speed of light and

$$\Theta = \omega_0 \tau \theta_0^2 \qquad (3\text{-}13)$$

is the rms angular beamwidth of the received signal. Θ_0 is the phase function width introduced above and τ is the optical thickness. ω_0 is the single scatter albedo:

$$\omega_0 = \frac{\alpha_s}{\alpha_a + \alpha_s} . \qquad (3\text{-}14)$$

One final point should be made about utilizing the multiple forward scatter theory with real phase functions, which typically have significant wide-angle scatter and backscatter components. Since, as stated above, it is a basic premise of the theory that these non-forward-scatter components are never collected by the receiver, they are lumped into absorption. Thus the actual scattering and absorption coefficients in the medium are scaled as follows:

$$\alpha_s' = \phi \alpha_s$$

$$\alpha_a' = \alpha_a + (1 - \phi)\alpha_s \qquad (3\text{-}15)$$

where ϕ is the forward scatter efficiency defined by

$$\phi = 2\pi \int_0^{\theta_F} P(\theta) \sin \theta d\theta \qquad (3\text{-}16)$$

θ_F is the effective width of the forward scatter peak. (There are various ways of determining θ_F. The method used here is that used in reference [17] The quantities α_a' and α_s' are used for computations with the theory instead of α_a and α_s.

3.2 Application to UV Experiments

In this   section, the theoretical results presented above will be used to compute the expected angular spreading for the conditions encountered in the uv field experiments. Comparisons will be made with the measured data. The three theories will also be used to predict the multipath

time spread expected under these conditions.

As a preliminary to these comparisons, subsection 3.2.1 will discuss the applicable phase functions needed for the computations.

3.2.1 Middle UV Phase Functions in Fog

The accuracy of single scatter and multiple forward scatter computations depends upon the use of an appropriate phase function. However, in most case of interest it is parameters such as the width and zero-angle peak value that are most important, while the specific shape is less important. Hence, a variety of different shapes are used (e.g., Henyey-Greenstein and Gaussian). As long as the free parameters in the proposed phase function are adjusted to embody the essential features of the physical situation, the results of the theory should be accurate.

As stated in Section 2.1, no particle size measurements were made during the uv experiments. Hence it is necessary to rely on published data for comparisons of theory with our experiments. Because of the relatively consistent weather conditions encountered during the experiments, a phase function for a stable maritime fog should be the appropriate one to use. However, no measurements of this type of phase function in the middle uv have been published. Reference [10] contains a measured fog phase function
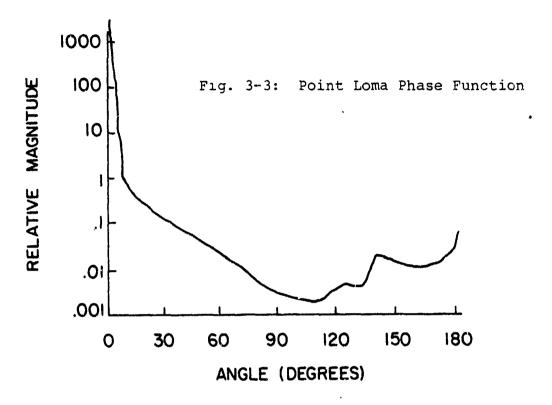
at a wavelength of 250 nm, but it is for a radiational (inland) fog. For the purposes of initial comparison, the phase function that will be used is that presented in reference [17], which is typical for 0.53μm propagation in maritime fogs at Point Loma, San Diego, California. (See Fig. 3-3.) Section 3.2.2 will include a discussion of how the theoretical results depend on the specific phase function parameters chosen.

For the Point Loma phase function, reference [17] gives the following values for the parameters ϕ, θ_0 and g:

$$\theta_0 = 11.3 \text{ mr}$$
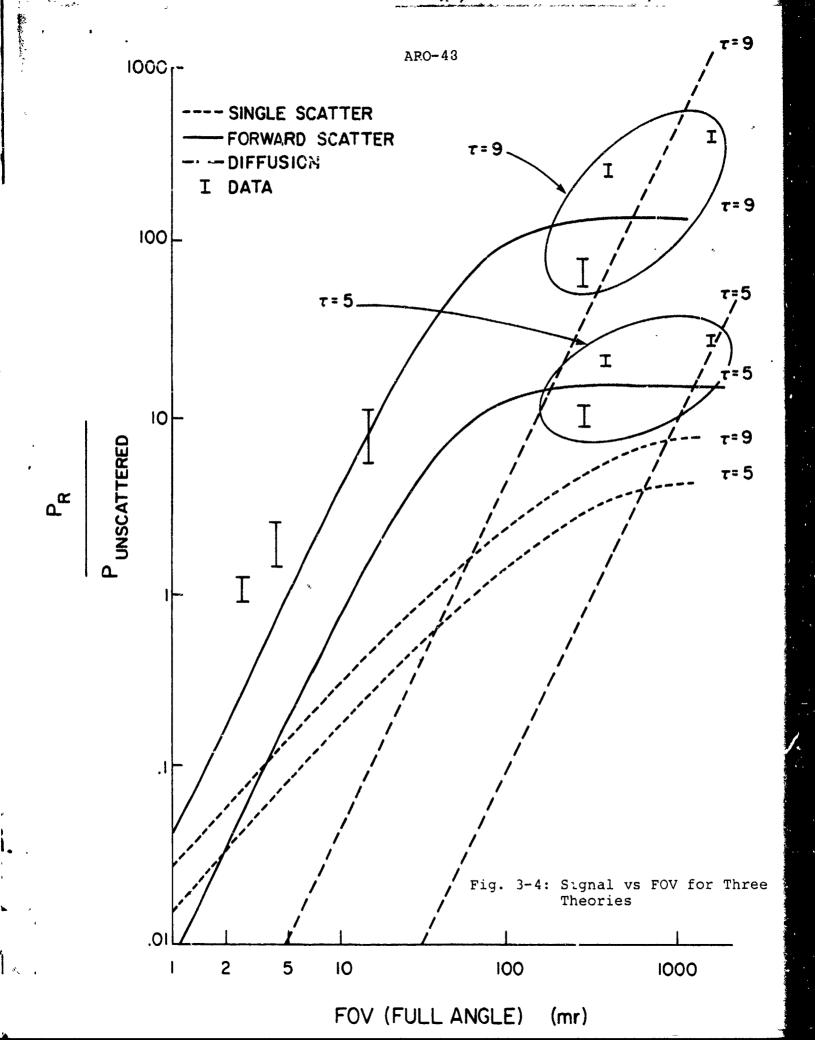
$$\phi = 0.57 \tag{3-16}$$

3.2.2. Angular spreading

This subsection uses the theories presented in Section 3.1 to predict angular spreading behavior for the experimental conditions encountered in

Fig. 3-3:   Point Loma Phase Function

Lubec and Eastport.

Measured and theoretical signal versus FOV characteristics are plotted in Fig. 3-4 for two values of ζ. The large FOV data is in two groups: the lower group of data represents $\zeta=5$ and the upper group $\zeta=9$. At small fields of view, the data was not very sensitive to changes in ζ; the entire range of values observed for $5 < \zeta < 9$ was included in the error bars. (This is consistent with Figs. 2-8 through 2-10, in which the slopes of the 5, 10 and 15 mr curves do not significantly differ.)   Note that since the actual signal versus FOV measurements included the unscattered component, this has been subtracted out of the data in the plot. Thus the data points represent purely scattered signal.

It is immediately evident upon inspecting Fig. 3-4 that both the diffusion component and the single scatter component are an order of magnitude below the measured data for fields of view less than 50 mr. The multiple forward scatter component for $\zeta=9$ is quite close to the measured data for

Fig. 3-4: Signal vs FOV for Three Theories

fields of view less than 15 mr, and both the $\tau=5$ and $\tau=9$ curves are close to the data at larger fields of view. One interestng feature of these curves is that while the multiple forward scatter component flattens out completely for angles greater than about 200 mr, the data appears to be increasing in that region. Note, however, that in both cases the diffusion component becomes significant at these large fields of view. Thus the measured large FOV behavior might be explained by a change in dominance from the multiple forward scatter component to the diffusion component.

The conclusion that diffusion and single scatter contribute a negligible amount to the small FOV received signal is quite insensitive to specific assumptions about the phase function. Fig. 3-5 shows the variation in the two characteristics as the parameter g is varied. The optical thickness is 5. It is clear from these curves that diffusion depends only minimally on the value of g. While the single scatter variations are more pronounced, the most extreme case is still below the unscattered component for fields of view less than 25 mr.

The variation in the multiple forward scatter component is somewhat more complicated because of the dependence on the two parameters θ_0 and ϕ. Re-writing Eq. (3-9) in terms of these parameters and dividing by the unscattered component, shows this dependence explicitly:

$$\frac{\langle P_d \rangle}{P_{unscattered}} = \frac{(FOV)^2 e^{\tau\phi\omega_0}}{5.48\theta_0^2\phi\tau + (FOV)^2} \qquad (3-17)$$

Here FOV is the full angle field of view and ω_0 is the scattering albedo. Observe that the exclusive role of θ_0 is to determine the breakpoint in the curve, while ϕ affects both the breakpoint (to a lesser extent than θ_0) and the final value (exponentially).

Figures 3-6 and 3-7 show multiple forward scatter signal versus FOV characteristic for various values of θ_0 and ϕ. Note from Fig. 3-6 that ϕ
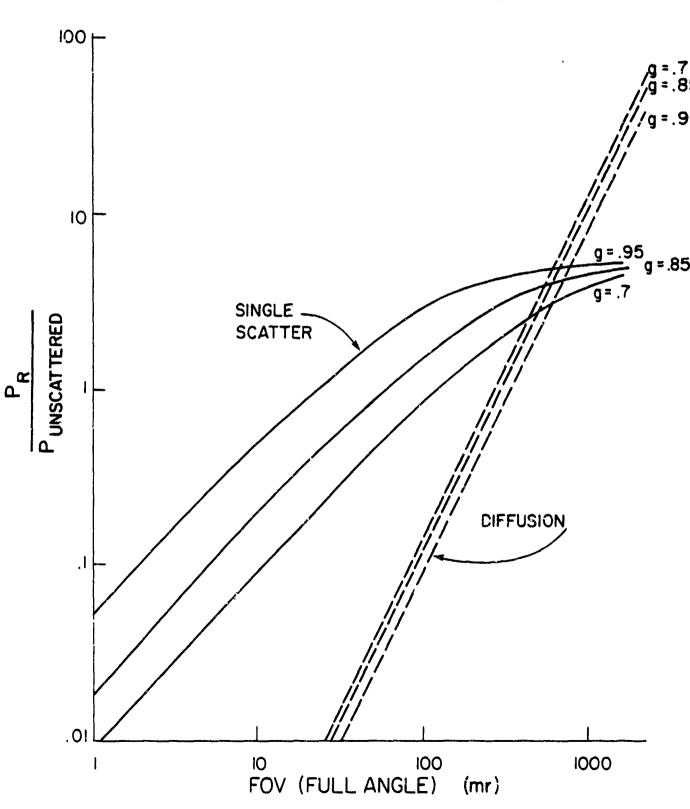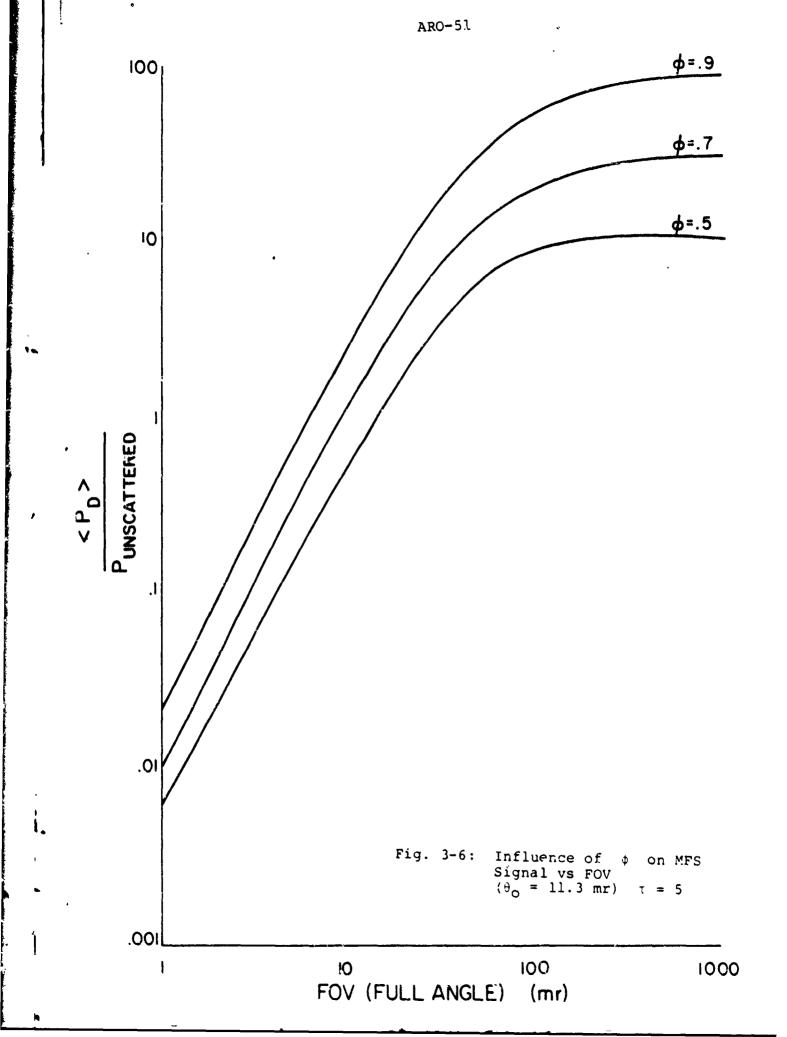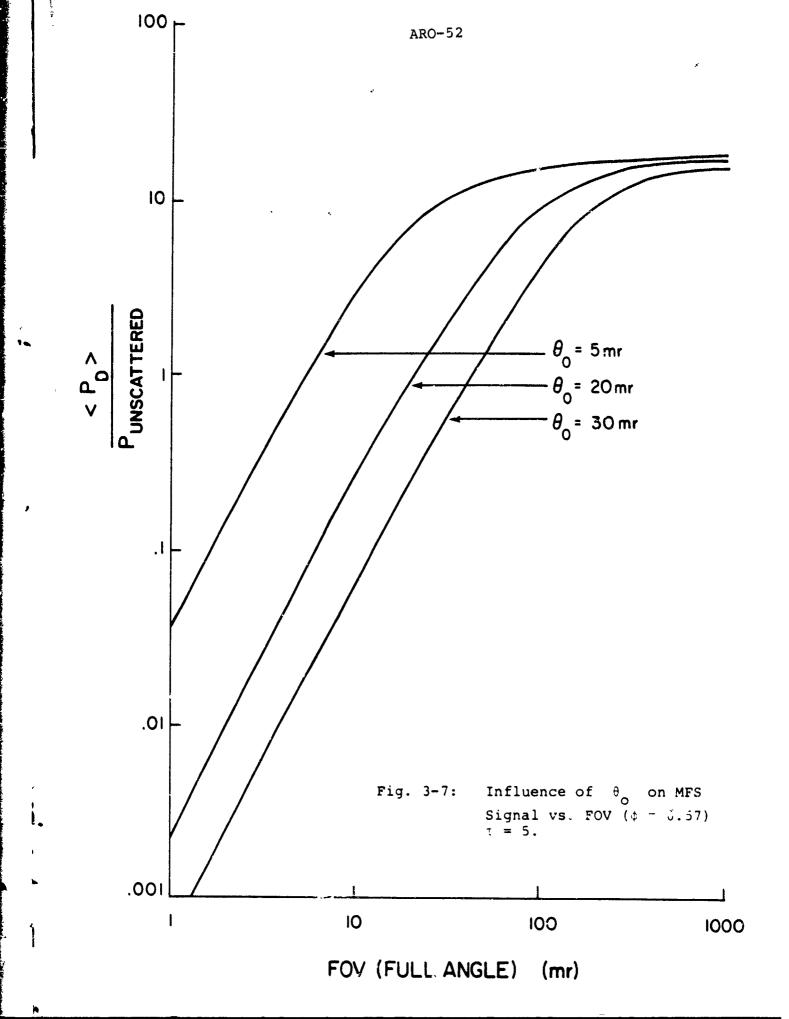
Fig. 3-5: Influence of Average Cosine
on Single Scatter and
Diffusion Results

Fig. 3-6: Influence of ϕ on MFS Signal vs FOV (θ_o = 11.3 mr) τ = 5

Fig. 3-7: Influence of θ_0 on MFS Signal vs. FOV ($\phi - 0.57$) $\tau = 5$.

does not significantly affect the small FOV behavior of the curve, although it changes the final value by almost an order of magnitude. From Fig. 3-7, however, it is clear that θ_0 drastically affects the small angle signal by changing the breakpoint of the curve. Because of this critical dependence on θ_0, it is difficult to say that the multiple forward scatter theory matches our experimental data. By appropriate choice of θ_0 and ϕ, the theory can be made to match a wide range of data. Thus, an accurate, independent determination of these parameters would be required to state with certainty that the theory is a good fit to the data.

On the other hand, the narrow forward angle peak of the fog phase function coupled with the observed narrowness of the angular spectrum, strongly recommends the multiple forward scatter theory or something similar. And, of course, of the three theories discussed, the multiple forward scatter theory is the only one that predicts anything like the observed behavior. It is, in fact, remarkable that with all the uncertainties involved in using the Point Loma phase function, the signal versus FOV characteristic for $\theta_0 = 11.3$ mr, $\phi = 0.57$ and $\tau = 9$ is reasonably close to the data for most fields of view observed.

One final remark is appropriate here before proceeding with the discussion of multipath time spread. If the multiple forward scatter component proves to be the dominant one for narrow receiver fields of view, this has certain implications for the difference between collimated and wide angle sources. In particular, it implies that the character of the received field is not significantly different for the two types of sources, since only light which remains confined to a small cone around the optical axis has a chance of reaching the receiver.

3.2.3 Multipath Time Spread Estimates

This section provides a brief discussion of multipath time spread and estimates of time spread are made for the experimental conditions encountered in the uv field trips.

In general, measured multipath time spread depends on receiver FOV as well as channel conditions. This is a consequence of the larger percentage of longer photon paths among those which make up the off-axis signal. This angular dependence varies among the different components of the field discussed above. On one extreme is the very explicit relationship between FOV and time spread in the single scatter component. For the coaxial geometry illustrated in Fig 3-1, the intersection of the transmitter and receiver cone angles sets an absolute upper limit to the time spread. On the other extreme is the diffusion component, which has no angular dependence.

Between these extremes is the multiple forward scatter component. Observe, however, that the time spread expression derived by Stotts [Eq.(3-12)] does not include any FOV dependence. Upon inspection of his derivation [27], it is evident that Eq. (3-12)applies to the situation in which the receiver FOV is large enough to collect all of the multiple forward scatter component. Hence, his expression gives an upper bound to the multipath time spread attributable to this component.

Table 3-2 shows computed values of time spread using the three theories. Bucher's simulation formula [20] is also included. The physical conditions assumed for these estimates are:

$$L = .31 \text{ km}$$

$$g = 0.85$$

$$\omega_0 = 0.96$$

$$\phi = 0.57$$

$$\theta_0 = 11.3 \text{ mr}$$

$$FCV \text{ (full angle)} = 100 \text{ mr}$$

The FOV is taken to be large enough so that the majority of the multiple forward scattered light is collected,

Table 3-2. TIME SPREAD ESTIMATES FOR 0.31 KM PATH (SEC)

γ	Single Scatter (FWHM)	MFS (rms)	Bucher (rms)	Diffusion (FWHM)
5	5×10^{-11}	1.31×10^{-8}	5.14×10^{-7}	$2.5-11.9 \times 10^{-7}$
7	5×10^{-11}	1.30×10^{-8}	6.77×10^{-7}	$3.6-16.5 \times 10^{-7}$
9	5×10^{-11}	1.31×10^{-8}	8.3×10^{-7}	$4.7-21.4 \times 10^{-7}$

Observe from the table that even in the worst case of diffusion, the multipath spread does not significantly exceed 2μsec. This is consistent with the lack of time spreading observed with the $1-2 \mu$sec pulsed source in the Eastport experiments for optical thicknesses less than 10.

4.0 Transport equation simplifications

One major purpose of the uv experiments has been to obtain enough information about the propagation parameters so that the transport equation can be simplified. In this section, we discuss one particular simplification, which results from the observed insensitivity of the scattered signal component to spatial variations in the medium's extinction coefficient (see Section 2.4). (Another simplification, based on the relative narrowness of the measured angular spectrum, is discussed elsewhere [23].) Specifically, it will be shown that under certain conditions only the homogeneous transport equation needs to be solved. The basic argument and result is presented here, but no detailed solutions are pursued.

Consider the generally spatially inhomogeneous linear transport equation [7,8]

$$\left(\alpha(\bar{r}) + \frac{1}{c} \frac{\partial}{\partial t} + \bar{\Omega} \cdot \bar{\nabla} \right) f(\bar{r}, \bar{\Omega}, t)$$

$$= \alpha_s(\bar{r}) \int d\bar{\Omega}' \, p(\bar{\Omega} \cdot \bar{\Omega}') \, f(\bar{r}, \bar{\Omega}', t),$$

where $f(\bar{r}, \bar{\Omega}, t)$ is the probability density of time t for a photon to be at point $\bar{r}$, going in direction $\bar{\Omega}$;

$\alpha(\bar{r})$ is the extinction coefficient at point $\bar{r}$ in the medium;

$\alpha_s(\bar{r})$ is the scattering coefficient at point $\bar{r}$ in the medium;

$p(\bar{\Omega} \cdot \bar{\Omega}')$ is the normalized single scattering phase function;

c is the speed of light;

∇ is the gradient operator.

Observe that the angular characteristics of the phase function are assumed to be the same throughout the medium: the inhomogeneity is lumped into the scattering coefficient $\alpha_s(\bar{r})$. Both $\alpha(\bar{r})$ and $\alpha_s(\bar{r})$ are random processes.

To simplify the subsequent discussion, it will be helpful to consider the integral equation corresponding to Eq(4-1) in the Laplace domain. Taking the one-sided Laplace transform of Eq (4-1) and integrating with respect to the pathlength variable in the direction

of photon travel gives

$$F(\overline{r}, \overline{\Omega}, s) = \int_0^\infty d \; \alpha_s(\overline{r} - \nu\overline{\Omega}) \int d\overline{}' p(\overline{\Omega}\cdot\overline{\Omega}') F(\overline{r} - \nu\overline{\Omega}, \overline{\Omega}', s)$$

$$(4-2)$$

$$\cdot \exp[-\int_0^\nu \gamma(\overline{r} - \nu'\overline{\Omega}) d\nu']$$

$$+ \frac{1}{c} \int_0^\infty d\gamma \; F_0(\overline{r} - \nu\overline{\Omega}, \overline{\Omega}) \exp[-\int_0^\nu \gamma(\overline{r} - \nu'\overline{\Omega}) d\nu'],$$

where

$$F(\overline{r}, \overline{\Omega}, s) = \int_0^\infty ds \; f(\overline{r}, \overline{\Omega}, t) \; e^{-st} \qquad (4-3)$$

$$\gamma(\overline{r}) = \alpha(\overline{r}) + s/c, \qquad (4-4)$$

and

$$F_0(r, \overline{\Omega}) = f(\overline{r}, \overline{\Omega}, t = 0), \qquad (4-5)$$

The second term in Eq (4-2) is a source term introduced by the initial value property of the one-sided Laplace transform. It corresponds to the unscattered component of the received field, and is denoted by $F_u(\overline{r}, \overline{\Omega}, s)$

The insensitivity property of the scattered field is now introduced in the following manner: Eq. (4-2) is converted to an integral equation for the scattered part of $F(\overline{r}, \overline{\Omega}, s)$, denoted by $F_s(\overline{r}, \overline{\Omega}, \overline{s})$. This is accomplished by substituting

$$F(\overline{r}, \overline{\Omega}, s) = F_u(\overline{r}, \overline{\Omega}, s) + F_s(\overline{r}, \overline{\Omega}, s) \qquad (4-6)$$

on both sides of the equation and cancelling common terms. The

result is:

$$F_s(r, \overline{\Omega}, s) = \int_0^\infty d\nu \, \alpha_s(\overline{r} - \nu\overline{\Omega}) \int d\overline{\Omega}' p(\overline{\Omega} \cdot \overline{\Omega}') F_s(\overline{r} - \nu\overline{\Omega}, \overline{\Omega}', s)$$

$$\exp[-\int_0^\nu \gamma(\overline{r} - \nu' \, \overline{\Omega}) \, d\nu']$$

$$+ \int_0^\infty d\nu \alpha_s(\overline{r} - \nu \, \overline{\Omega}) \int d\overline{\Omega}' \, p(\overline{\Omega} \cdot \overline{\Omega}') F_u(\overline{r} - \nu\overline{\Omega}, \overline{\Omega}', s)$$

$$\exp[-\int_c^\nu \alpha(\overline{r} - \nu'\overline{\Omega}) d\nu']. \qquad (4-7)$$

The first term in Eq (4-7) is the multiple scatter portion of $F_s(\overline{r}, \overline{\Omega}, s)$ and the second term is the single scatter portion.

It can be shown that under certain conditions, the second term in Eq (4-7) has the same dependence on the variations in $\alpha(\overline{r})$ as does the unscattered component itself. This implies that this term must be small compared to the first term since the left hand side of Eq (4-7) must be insensitive to these variations. Furthermore, the first term must also be insensitive to these variations, so that it must behave nearly as if its randomly space-varying extinction and scattering coefficients were replaced by their means. Hence, Eq. (4-7) can be written as

$$F_s(\overline{r}, \overline{\Omega}, s) = <\alpha_s> \int_0^\infty d\nu \int d\overline{\Omega}' p(\overline{\Omega} \cdot \overline{\Omega}') F_s(\overline{r} - \nu\overline{\Omega}, \overline{\Omega}', s) e^{-<\alpha>\nu}$$

$$(4-8)$$

(Two basic assumptions are implicit in this argument: first, that there is no exotic form of cancellation occurring between the single and multiple scattering terms; and second, that the first term is not the small term, i.e., this is not simply a single scatter problem.)

Sufficient conditions for Eq (4-8) to be valid are:

1) $\overline{\Omega}$ is not vaery far off the optical axis $(\overline{\Omega} \cdot \frac{\overline{r}}{|\overline{r}|} \approx 1)$;

2) $p(\overline{\Omega} \cdot \overline{\Omega}')$ has a pronounced forward peak $(p(90°) << p(0°))$.

The second condition is not very restrictive, and is satisfied by all for phase functions (see Fig. 3-3). The first condition is quite restrictive, but we believe it can be relaxed. On general physical grounds, it can be argued that the further off axis the receiver looks, the more the light it collects will be dominated by multiple scatter.

Furthermore, the experimental evidence (see Fig. 3-4 and 3-5) is consistent with this argument. Hence it is reasonable to assume that Eq (4-8) is valid for any $\overline{\Omega}$.

If the spatial Fourier transform

$$\tilde{F}_s(\overline{\omega}, \overline{\Omega}, s) = \int d\overline{r}\ F_s(\overline{r}, \overline{\Omega}, s) e^{-j\overline{\omega}\cdot\overline{r}} \tag{4-9}$$

is introduced into Eq (4-8), the integral over ν can be carried out, resulting in

$$\tilde{F}_s(\overline{\omega}, \overline{\Omega}, s) = \frac{<\alpha_s>}{<\gamma> + j\overline{\omega}\cdot\overline{\Omega}} \int d\overline{\Omega}'\, \rho(\overline{\Omega}\cdot\overline{\Omega}')\tilde{F}_s(\overline{\omega}, \overline{\Omega}', s). \tag{4-10}$$

Eq. (4-10) is the desired result. It is a singular eigenfunction equation for $\tilde{F}_s(\overline{\omega}, \overline{\Omega}, s)$. Although time has not been available to explore solutions of Eq(4-10), it is essentially identical to one considered by Case and Zweifel [7]. The lack of the source term is a significant simplification over the original transport equation, and may afford closed form solutions for physical conditions under which the assumptions leading to Eq(4-10) apply.

References

1. D. M. Reilly, "Atmospheric Optical Communications in the Middle Ultraviolet", M. S. Thesis, Department of Electrical Engineering and Computer Science, MIT, May 1976.

2. R. S. Kennedy, "Communication through Optical Scattering Channels: An Introduction", Proc. IEEE, Vol. 58, No. 10, October 1970, pp. 1651-1665.

3. R. M. Lerner and A. E. Holland, "The Optical Scatter Channel", Proc. IEEE, Vol. 58, No. 10, October 1970, pp. 1547-1563.

4. W. S. Ross, "An Investigation of Atmospheric Optically Scattered Non-Line-of-Sight Communication Links", First Year Final Report, US ARO Contract DAAG29-77-C-0048, September 26, 1978.

5. T. T. Nguyen, "Automated Signal vs. Field of View Measurement in the Middle Ultraviolet" B.S. Thesis, Department of Electrical Engineering and Computer Science, MIT, May 1979.

6. J. H. Shapiro, "The Extended Huygens-Fresnel Principle," Internal Paper, Optical Propagation and Communication Group, Research Laboratory of Electronics, MIT, March 5, 1979.

7. K. M. Case and P. F. Zweifel, Linear Transport Theory, Addison Wesley, Reading, Mass. 1967.

8. K. M. Case, F. de Hoffmann, G. Placzek, Introduction to the Theory of Neutron Diffusion, Los Alamos Scientific Laboratory, Los Alamos, New Mexico, June 1953.

9. D. Deirmendjian, Electromagnetic Scattering on Spherical Polydispersion, American Elsevier, New York, 1969.

10. M. E. Neer, et al, "Atmospheric Propagation of Ultraviolet Radiation through the Lower Atmosphere", Aeronautical Research Associates of Princeton, Report No. 374b, November 1978.

11. D. Ludlum, et. al, New England Weather Book, Houghton Mifflin, Boston, 1976, p. 78.

12. R. Rhine, "Fog Data for the Lubec-Campobello-Eastport Area from January 1, 1959-April 26, 1979", excerpted from the records of U.S. Climatological Service Station #17-N-50-1226-1, North Lubec, Maine.

13. E. J. McCartney, Optics of the Atmosphere, John Wiley and Sons, New York, 1976.

14. R. C. Eldridge, "Haze and Fog Aerosol Distributions", Journal of the Atmospheric Sciences, Vol. 23, September 1966.

15. S. V. Sperry, Propagation of Ultraviolet Light Through the Lower Atmosphere", M. S. Thesis, Department of Electrical Engineering and Computer Science, MIT, February 1978, p. 13.

16. H. M. Heggestad, Optical Communication Through Multiple Scattering Media, Technical Report No. 472, Research Laboratory of Electronics, MIT, November 1968.

17. G. C. Mooradian, et. al., "Blue-Green Pulsed Propagation Through Fog", Applied Optics, Vol. 18, No. 4, February 15, 1979, pp. 429-441.

18. D. M. Reilly and C. Warde, "Temporal Characteristics of Single Scatter Radiation", JOSA, Vol. 69, No. 3, March 1979, pp. 464-470.

19. R. S. Kennedy, Atmospheric Optical Communication, to be published by Office of Telecommunications, US Department of Commerce.

20. E. A. Bucher, "Computer Simulation of Light Pulse Propagation for Communication through Thick Clouds", Applied Optics, Vol. 12, No. 10, October 1973, pp. 2391-2400.

21. R. W. Preisendorfer, Hydrologic Optics, Volume 3, Solutions, US Department of Commerce, National Oceanic and Atmospheric Administration, 1976, pp. 175ff.

22. A. Ishimaru, Wave Propagation and Scattering in Random Media, Volume 1, Academic Press, New York 1978, chap. 13.

23. R. S. Kennedy, and J. H. Shapiro, "Multipath Dispersion in Low Visibility Optical Communication Channels", Final Report, Contract No. F19628-76-C-0054 for Rome Air Development Center, Hanscom Air Force Base, Bedford, Mass., January 1977.

24. W. H. Paik, et. al., "Propagation Experiments in Low Visibility Atmospheres," Applied Optics, Vol. 17, No. 6, March 15, 1978, pp. 899-905.

25. E. A. Bucher, "Propagation Models for Optical Communication Through Fog and Clouds," Proceedings of the National Electronics Conference, Chicago, October 16-18, 1974, pp. 180-185.

26. J. H. Shapiro, "Imaging and Optical Communication through Atmospheric Turbulence", in Laser Beam Propagation in the Atmosphre, Springer-Verlag, Berlin, 1978, chap. 6.

27. L. B. Stotts, "Closed Form Expression for Optical Pulse Broadening in Multiple-Scattering Media", Applied Optics, Vol. 17, No. 4, February 15, 1978, p. 504.

28. W. A. Baum and L. Dunkelman, "Horizontal Attenuation of Ultraviolet Light by the Lower Atmosphere", JOSA, Vol. 45, No. 3, March 1955, pp 166-175.

29. E. P. Shettle, "Effects of Humidity Variations on Atmospheric Aerosol Optical Properties," Preprint Volume: Third Conference on Atmospheric Radiation, June 28-30, 1978, Davis, California, pp 231-233.